IEEE Access
Multidisciplinary | Rapid Review | Open Access Journal

Received 30 April 2024, accepted 19 May 2024, date of publication 27 May 2024, date of current version 3 June 2024.

Digital Object Identifier 10.1109/ACCESS.2024.3406219

RESEARCH ARTICLE

Real-Time Experimental Evaluation and Analysis of PID and MPC Controllers Using HIL Setup for Robust Steering System of Autonomous Vehicles

S. GOKUL KRISHNAN[1], P. SURESH KUMAR[2], NADHEEM NASSAR MATARA[3], AND YONG WANG[4]

[1]School of Electrical Engineering, Vellore Institute of Technology, Vellore 632014, India
[2]Automotive Research Centre, Vellore Institute of Technology, Vellore 632014, India
[3]Department of Automotive Engineering, Vellore Institute of Technology, Vellore 632014, India
[4]Department of Systems Science and Industrial Engineering, Binghamton University, Binghamton, NY 13902, USA

Corresponding author: P. Suresh Kumar (suresh.kumar@vit.ac.in)

ABSTRACT The development of autonomous vehicles has recently received substantial impetus, fueled by researchers and industry personnel. The need for powerful steering control in autonomous vehicles is critical for assuring the vehicle's safety and reliability. Robust steering control allows for precise and accurate maneuvering, allowing the vehicle to traverse complicated road conditions. Comparative research on the certification of a robust steering system for autonomous vehicles is presented in this paper. Traditional controllers (PD and PID) are compared with a modern Model Predictive Control (MPC) controller that uses a multi-turn potentiometer and incremental encoder for position feedback. The controllers are designed in MATLAB Simulink and deployed for real-time testing on a Speedgoat performance real-time target Hardware-in-the-Loop (HIL) machine. The study focuses on evaluating the steering system's real-time performance in terms of accuracy and robustness. The novelty is that this work is carried out in a real experimental modified electric vehicle and presents real-time results obtained using the HIL machine and Rapid Control Prototyping (RCP) technique. The research covers a thorough examination of the experimental hardware configuration, system identification, controller design, and data-gathering technologies. A significant contribution of this research is the use of the HIL machine for real-time performance testing of different controllers with different velocities and sample times, specifically in a speed breaker scenario. To analyze each controller's response, real-time data is logged at a high sampling rate of 0.1 milliseconds. The research contributes to the advancement of driverless vehicles by providing insights into the optimal performance of steering systems. It also emphasizes the importance of real-time testing of the robust performance of different controllers to ensure human safety in driverless cars.

INDEX TERMS Steering system, autonomous vehicle, model predictive control (MPC), rapid control prototyping (RCP), hardware-in-the-loop (HIL), robust control.

NOMENCLATURE

PARAMETERS

K_p - Proportional Gain.
K_i - Integral Gain.
K_d - Derivative Gain.
N - Filter Coefficient.
$u(t)$ - Output of PID Controller.
$U_t^*(x(t))$ - Output of MPC Controller.
J - Cost Function.
Nc - Control Horizon.

The associate editor coordinating the review of this manuscript and approving it for publication was Ton Duc Do.

Np - Prediction Horizon.
Ts - Sample Time.

ABBREVIATIONS

CNN - Convolution Neural Network.
EPS - Electric Power Steering.
HIL - Hardware-in-the-Loop.
I/O - Input Output.
IC - Internal Combustion.
LQR - Linear Quadratic Regulator.
MPC - Model Predictive Controller.
PD - Proportional-Derivative.
PID - Proportional-Integral-Derivative.
PWM - Pulse Width Modulation.
RCP - Rapid Control Prototyping.
TTL - Transistor-Transistor Logic.

I. INTRODUCTION

The development of autonomous ground vehicles, also referred to as self-driving cars or autonomous vehicles, has significant implications and potential applications in future smart and sustainable transportation. It is a very crucial turning point in transportation, with implications for safety, efficiency, accessibility, and environmental sustainability. The ability to improve road safety is one of the key benefits of autonomous ground vehicles. Human distractions are the major source of accidents, and autonomous cars can reduce or eliminate them by utilizing modern sensors, artificial intelligence, and real-time data processing. Autonomous vehicles, by reducing the need for human drivers, have the potential to reduce accidents and save lives. Furthermore, self-driving ground vehicles have the potential to improve transportation efficiency. Because they can communicate with other vehicles and with the infrastructure, these cars can optimize routes, minimize traffic congestion, and reduce fuel use.

The autonomous vehicle steering system can improve safety, by eliminating driver errors. Its performance majorly depends on the sensor's resolution and its range. The autonomous vehicle system receives feedback information from LiDAR, radar, camera, steering angular position, and velocity measurement sensors. Robust steering control in autonomous vehicles is critical to guarantee the safe and reliable functioning of self-driving cars. The capacity of an autonomous vehicle to regulate its steering inputs reliably and precisely in a variety of complex environmental conditions is referred to as robust steering control. Improved safety is one of the key advantages of precise steering control. Autonomous vehicles must be capable of dealing with unforeseen scenarios such as unexpected barriers, unpredictable weather, or complex road terrains. Robust steering control enables the vehicle to respond rapidly and efficiently to these situations, assisting in collision avoidance and ensuring the safety of passengers, pedestrians, and other vehicles on the road. A robust steering control system provides better performance for driver-less cars, in the presence of difficult road conditions like uneven terrain, slippery roads, speed breakers, potholes, heavy rain and snow.

In recent literature, different types of Model Predictive Control (MPC) controllers are used for autonomous vehicle robust steering control systems. The design of the MPC controller that utilized lateral and steering angle deviation, along with relative yaw angle to control steering angle for collision avoidance based on the LiDAR data is presented in [1]. MPC controller is used to compensate the side slip for improving the tracking performance for higher speeds [2], and its performance is evaluated based on the actuator's bandwidth [3]. A linear model-based path tracker using an MPC controller by linearizing the sequence of future steering angles has been discussed [4]. Three different types of algorithms like Ziegler-Nichol's, WAF-tune, and twiddle are used to tune the PID controller gains to improve the steering performance [5].

To ensure safe cooperation between humans and machines, several studies have proposed various methods to enhance autonomous vehicle steering performance. A model reference adaptive control approach is proposed by [6] to ensure cooperation between humans and machines, which will give robust performance for disturbances. A methodology for ensuring a smooth transition between autonomous steering control and driver input for low and high-speed maneuvers is given in [7]. Small-gain theory and an iterative scheme to learn and adapt to the driver's steering torque, to jointly operate the vehicle is analyzed in [8].

The design and development of an MPC controller for high-speed accident avoidance is proposed in [9]. A hierarchical control architecture that consists of a decision-making layer and a motion control layer, is validated with hardware-in-the-loop (HIL) testing. Reference [10] presented a new strategy that combines differential braking with autonomous steering for collision avoidance using an MPC controller to track the center line of the road and end the swerving maneuver is discussed in detail. In case of steer-by-wire system failure, [11] proposed a torque vectoring system in conjunction with the VSC system as a redundant measure to ensure the safety of the autonomous collision avoidance system. Takagi-Sugeno (T-S) fuzzy model based on a fuzzy Lyapunov control framework for automatic lane keeping under varying system constraints such as unknown crosswinds and varying road curvatures is presented in [12]. Artificial neural networks such as Convolution Neural Network (CNN) and Long-Short-Term-Memory Network are used to predict the steering angle for lane keeping even during poor visibility conditions [13]. A novel algorithm is proposed for automated lane changing using yaw rate, steering angular position, and steering wheel feedback torque from the electric power steering (EPS) system [14].

A precise path-tracking control algorithm is proposed to accommodate varying vehicle weight, weight distribution, and velocity [4]. An optimal feedback controller is used

to handle the tracking errors and a feedforward controller is used to anticipate upcoming road turns to improve the autonomous vehicle steering tracking performance [5]. A trajectory tracking algorithm is analyzed in [15], using an MPC controller by considering a nonlinear multi-input and multi-output system with independent wheel steering capability. The adaptive steering controller [16] performance of MPC for autonomous vehicle steering systems is presented in [17].

Addressing trajectory planning for autonomous vehicle docking, [18] introduced an algorithm to determine the optimal path for seamless docking. Reference [19] compared the performance of Linear Quadratic Regulator (LQR) and MPC controllers in various scenarios, such as lane changing, perpendicular parking, and parallel parking, using a HIL system. Reference [20] presented an autonomous vehicle steering controller that utilizes an MPC controller to track the desired path, considering disturbances and time-varying parameter uncertainties. Reference [21] proposed a precise trajectory tracking control algorithm suitable for network delay in autonomous vehicles. To address vehicle stability regarding longitudinal velocity and mass, [22] designed an H-infinite robust controller that applies direct yaw moment control and active front steering control. Reference [6] developed a model reference adaptive controller capable of achieving robust performance despite disturbances and parameter uncertainties. [23] provided an insightful analysis of reference path-tracking control strategies and the advantages and limitations of robust and observer-based control strategies. Reference [24] contributed to this field by presenting robust control policies. In the context of lateral dynamics stability during maneuvers like single lane changes and J-turns, [25] proposed an adaptive backstepping control technique that effectively handles external disturbances and parameter uncertainties. Furthermore, [26] developed an adaptive two-layer control framework for a two-axle autonomous bus to prevent sideslips and rollovers, prioritizing safety, [27] designed a digital twin for safety system of an electric vehicle where several test scenarios can be simulated by tweaking many system parameters to observe the system state.

These recent studies have significantly advanced the field of autonomous vehicle control, incorporating deep reinforcement learning, trajectory planning, robust control algorithms, adaptive control techniques, and various control strategies to enhance vehicle performance, safety, and stability. Most of the above works are carried out in a simulation platform or a constrained experimental setup.

The novel highlights of this paper are,

- The physical vehicle is converted to a testbed and the experiment is performed in the actual situational cases for the evaluation of developed modern controllers using the HIL machine for real-time control and data acquisition which overcomes the limitations of other works enclosed.
- This paper is also focused on the work of precise and accurate maneuvering in complex and challenging road conditions for autonomous vehicle safety and reliability with the evaluation of the real-time performance of a robust controller using HIL testing.
- A comparative study is also carried out in this paper to validate a robust steering system for autonomous vehicles by comparing traditional controllers (PD and PID) with a modern Model Predictive Control (MPC) controller.

The study utilizes a multi-turn potentiometer and incremental encoder for position feedback. Performance tests at different velocities and sampling times, particularly in a speed breaker scenario, have been conducted.

The rest of this paper is organized into four sections. The following Section II describes the hardware experimental setup with the data acquisition system. Section III discusses the system identification and design of various controllers for steering system. Section IV provides the real-time experimental results that are obtained for the various test scenarios. Finally, the conclusion of the paper is presented in Section V.

II. EXPERIMENTAL SETUP

The complete test setup utilized a 7-seater Maruti Suzuki Versa car, equipped with a Speedgoat HIL machine and a high-performance PC. This setup incorporated the high-resolution 3D HDL-32E and VLP-16 Velodyne LiDARs, along with the Intel D435 depth camera. These sensors were employed for the perception, planning, and control of autonomous vehicles. Fig. 1 illustrates the autonomous vehicle with the speed breaker being examined and Fig. 2 shows the line diagram of the experimental setup. The test bench setup in the vehicle is shown in Fig. 3. Furthermore, this section covers the traction setup, steering setup, specifications of the HIL machine, data acquisition, noise removal, and filtering methods.

A. TRACTION SETUP

A separately excited DC motor is used as a traction motor with the specifications given in Table 1. The Kelly KDH12801E motor driver serves to manage the armature supply of the motor. The field supply is maintained at a steady 12V, facilitated by a 72V to 12V DC-DC converter. A Li-Ion battery pack, specified in Table 2, is utilized to fuel the vehicle. The schematic diagram of the car is depicted in Fig. 4. For precautionary measures, kill switches are affixed on each side of the car. Moreover, a 72V DC to 220V AC inverter caters to the power needs of the onboard desktop units, and a 220V AC to 12V DC converter provides for the vehicle's low-voltage systems.

B. STEERING SETUP

The vehicle features a standalone EPS system, employing a 12V DC brushed clutch motor. This motor is rerouted and

FIGURE 1. Autonomous car in front of the test speed breaker.

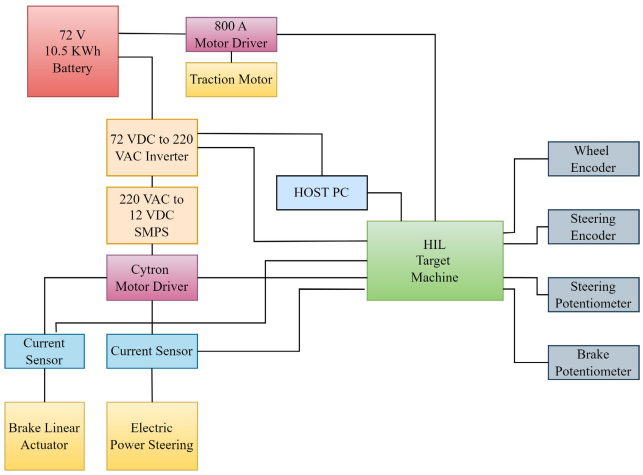

FIGURE 2. Line diagram of the experimental setup.

TABLE 1. Motor specifications.

Description	Value
Motor Power Rating	10kW
Motor Armature Voltage	72V
Motor Field Voltage	36V
Motor Torque	23Nm

TABLE 2. Battery specifications.

Description	Value
Battery Power Rating	3.3kW
Battery Capacity	46Ah
Battery Configuration	20s20p
Battery Nominal Voltage	72V
Battery Maximum Voltage	84V
C Rating	1.4C

linked to a Cytron MDDS30 motor driver. It is supplemented with an incremental encoder, boasting a resolution of 1024 pulses per revolution, mounted on the steering column. Moreover, a multiturn 10 kΩ potentiometer, geared to the steering, facilitates the measurement of the steering position via voltage conversion. The installation of the encoder and the potentiometer are depicted in Fig. 5 (a) and (b), respectively.

TABLE 3. Target hardware specifications.

Description	Value
CPU	Intel Core i7 4.2GHz, 4 cores
Memory (RAM)	4 GB DDR4
Main Drive	1 TB SSD
PCIe	IO133

C. HARDWARE-IN-THE-LOOP (HIL) MACHINE SETUP

All designed control algorithms are dispatched to a hardware system for real-time testing. For rapid control prototyping, we have utilized the Speedgoat performance real-time target machine, with its specifications detailed in Table 3. This robust machine carries out computations, actuation, and data acquisition in real-time. It interfaces directly with MATLAB Simulink version 2022b using the Simulink Real-Time Target Packages.

IO133 is a sophisticated analog input and output module (I/O), featuring 16 simultaneous-sampling analog input channels with 16-bit resolution, and 8 analog output channels with concurrent update and 16-bit resolution. Additionally, it possesses 14 configurable digital I/O pins for Transistor-Transistor Logic (TTL). It is predominantly utilized for rapid control prototyping and HIL testing, as displayed in Fig. 6(a). The module manages a traction motor through an analog output ranging from 0 - 5V; with 0V indicating no power flow and 5V representing the maximum power supply to the traction motor. The steering motor operates through a driver configured for 0 to 100% Pulse Width Modulation (PWM). A 50% duty cycle leaves the steering motor stationary, while alterations to 0% and 100% trigger anti-clockwise and clockwise rotations respectively. The PWM signal to the driver is dispatched via the HIL target machine utilizing the IO133 module. Feedback from the steering position is collected through a potentiometer, translating to an analog value of 0 - 5V, wherein 2.427V corresponds to the steering wheel's central position. This data is fed into the target machine using the IO133 module's analog input lines. Furthermore, the system interfaces with an incremental encoder, linking its A and B pulses to the digital I/O lines of the IO133 module within the target machine. The arrangement of the HIL machine setup can be seen in Fig. 6(b).

D. DATA ACQUISITION FROM STEERING MOUNTED POTENTIOMETER AND ENCODER

The wiper pin of the steering's potentiometer and the signal pins A and B of the steering's encoder are connected to the Speedgoat HIL machine, which serves as a data

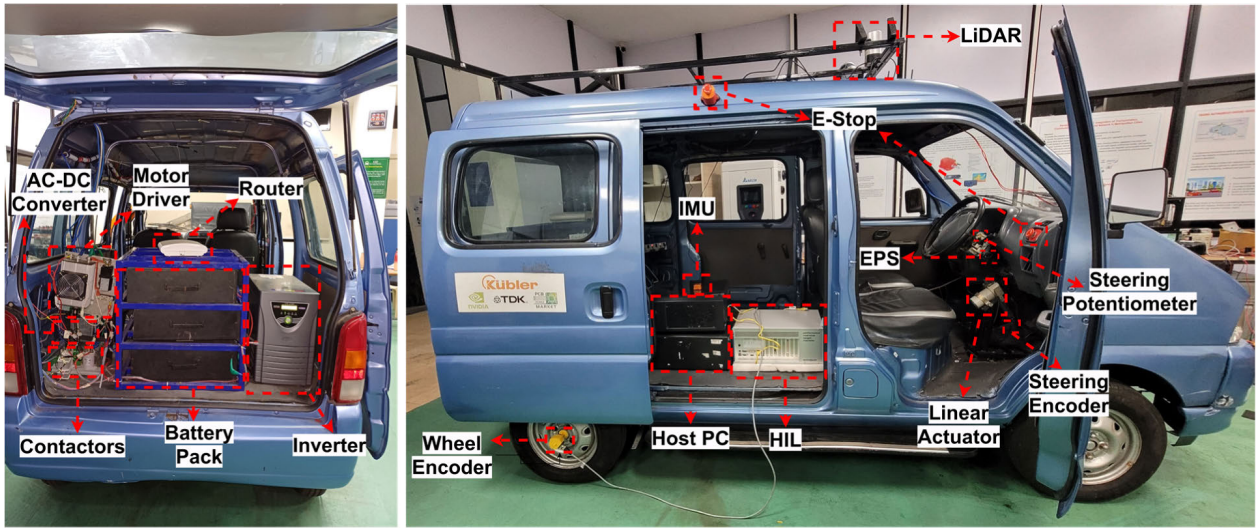

FIGURE 3. Experimental test bench setup in a real modified electric car.

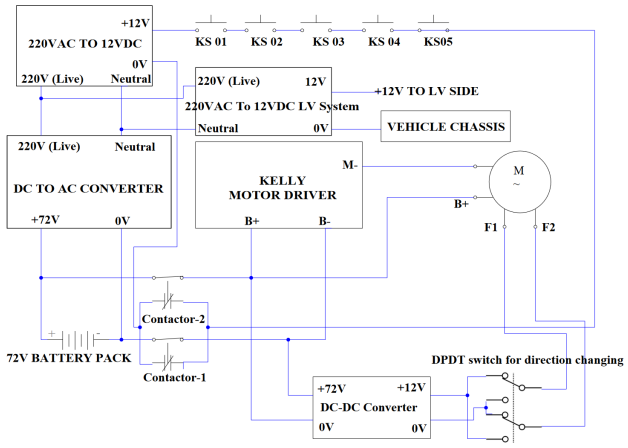

FIGURE 4. Circuit diagram of HV side of the vehicle.

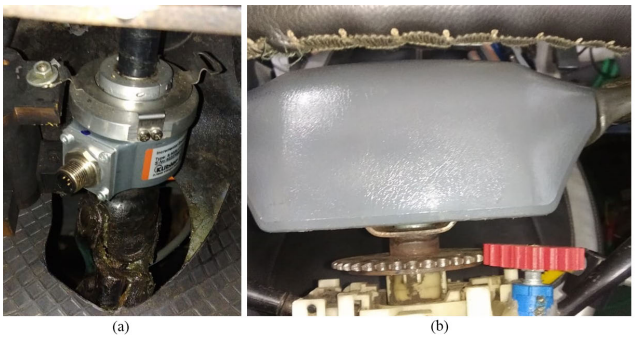

FIGURE 5. Steering angular position acquisition sensors.

acquisition device. A Simulink model is created, and the data is acquired using MATLAB Simulink's data inspector toolbox. To decode the encoder's data, a pre-built block called the quadrature shaft decoder is utilized, which converts the

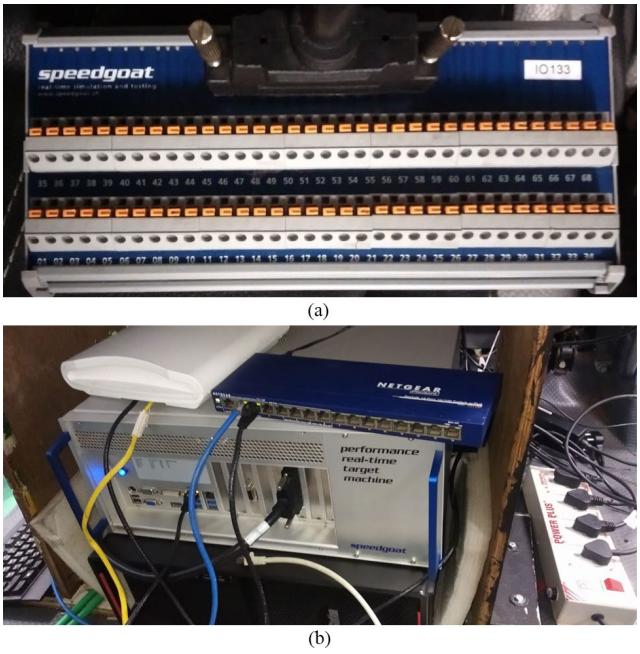

FIGURE 6. Connection from the HIL machine setup.

A and B encoder pulses into radians. The linear property of the potentiometer is employed to map the analog voltage of the potentiometer to radians. For manual measurement, the analog voltage corresponding to the zero radians position is recorded as 2.427V, and the analog voltage for a full right turn of the steering is measured as 0.299V, which corresponds to 16.638 radians. By establishing a straight-line equation between these two points, we determine the relationship between the analog voltage and the steering's position.

E. DATA FILTERING AND NOISE REMOVAL

The raw data that is directly obtained from the sensor consists of a lot of noises due to the surrounding electrical interference

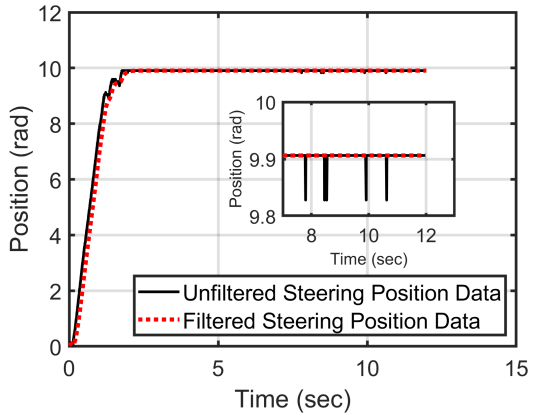

FIGURE 7. Connection from the HIL machine setup.

as unprocessed, unfiltered data that is shown in Fig. 7 The noise component is the data will spoil the signal quality and will have a great impact in the accuracy of the signal. The raw data should be filtered before using it for processing in the control system application. A generalised low pass filter with a cut-off frequency of 10 rad/sec has been designed as a transfer function model which is given by Eq. (1). The raw data from the steering block is fed to it as an input and the filtered noise-less data has been obtained as an output of the transfer function.

$$\frac{1}{0.1s+1} \tag{1}$$

III. METHODOLOGY

A. SYSTEM IDENTIFICATION

System identification involves the mathematical modeling of a dynamic system by establishing a relationship between its input and output. This process includes acquiring data for the input and output signals, selecting an appropriate model structure, estimating the system model using various techniques, and evaluating the accuracy of the obtained model. Obtaining the system model through first-principles modeling can be challenging as the mathematical parameters of a pre-designed system are difficult to determine. The strategy outlined in this work is regarded as a black box technique since it does not require knowledge of the system's physical dynamics. The system identification toolbox in MATLAB Simulink has a basic feature that allows researchers to tune the model's parameters until the model's output closely matches the observed output. The flowchart in Fig. 8 depicts the processes taken to obtain the system model.

1) STEERING SYSTEM DYNAMICS MODELING

The transfer function of a system represents the mathematical relationship between the input and output. In this case, the input is a voltage supply ranging from −12V to 12V, which is applied to the electric steering motor connected to the steering column. A voltage of −12V causes the steering to rotate counterclockwise, while 12V rotates it clockwise,

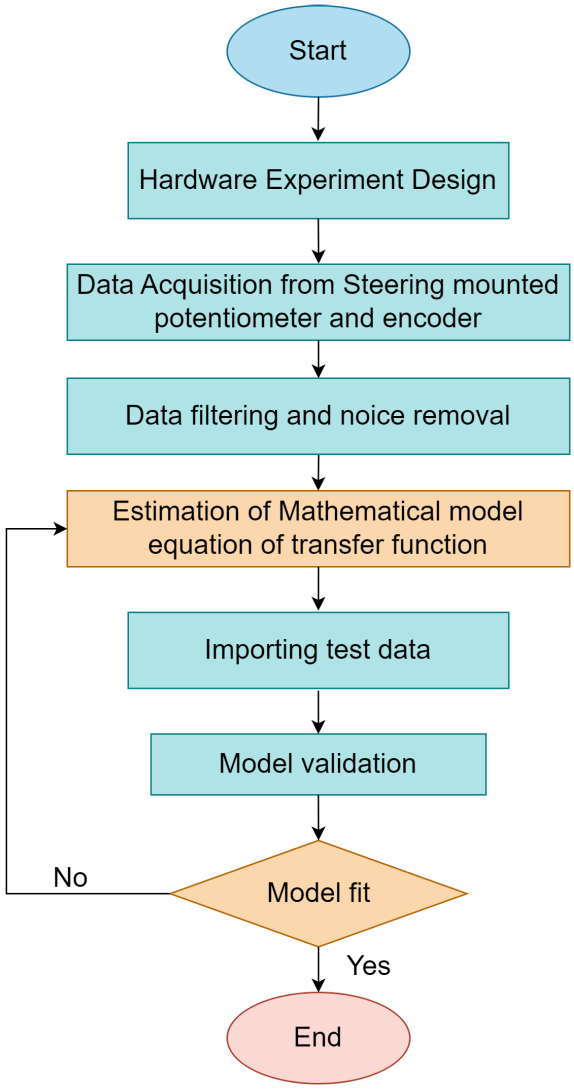

FIGURE 8. Flowchart of the system model design.

with 0V representing the rest position. The output of the system is the position of the steering in radians. To obtain the transfer function, MATLAB's system identification toolbox is used to analyze the input and output data. The frequency response modeling using the chirp signal [28] method is chosen for its ability to provide rapid stability and transient response information. Sinusoidal voltages with frequencies ranging from 0.75 rad/sec to 1.5 rad/sec and a peak-to-peak voltage of −12V to 12V are used as inputs to the system. Both distinct frequency modeling and multi-frequency modeling are performed using the same data set in the system identification toolbox. Fig. 9 shows the graph depicting the relationship between the input voltage and angular position of the steering system for frequencies ranging from 0.75 rad/sec to II rad/sec. The transfer function parameters for the multi-frequency modeling, obtained from MATLAB's system identification toolbox are the gain of the system k=4.730, damping ratio ζ=3.648 and the undamped

natural frequency ω_n=1.119. These parameters are plugged into the Eq. (2) to get the final transfer function of the system as given in Eq. (3).

$$\frac{\theta(s)}{V(s)} = \frac{{\omega_n}^2 k}{s^2 + 2\zeta\omega_n s + \omega_n^2} \tag{2}$$

$$\frac{\theta(s)}{V(s)} = \frac{5.922}{s^2 + 8.164s + 1.252} \tag{3}$$

where $\theta(s)$ represents the angular position of the steering system, and $V(s)$ represents the steering motor's input voltage.

2) MODEL VALIDATION

Model validation plays a critical role in ensuring the accuracy, completeness, and cleanliness of the obtained system model. It is crucial to validate the system model to design the controller with the desired specifications. The obtained system model should be tested using multiple different data sets to assess its validity, and it should demonstrate decent and acceptable accuracy. If the model performs with good accuracy and the model fit is satisfactory with the test and validation sets, then it can be considered final for further system processing. However, if the obtained model fails to perform well or lacks a good model fit, the estimation of the mathematical model equation, specifically the transfer function, should be repeated while increasing the order of the system. The obtained transfer function model as shown in the Eq. (3) is verified with 2 different test data known as the validation data set. The results show 78.65% as the best fit for the system.

B. CONTROLLER DESIGN

1) DESIGN OF PD AND PID CONTROLLER

PID controllers are widely used in the field of control engineering for regulating dynamics of the systems. They are renowned for their simplicity, effectiveness, and versatility in a wide range of applications. The developed system model utilized the transfer function toolbox in Simulink. The output from the PID controller block set serves as the input to the transfer function. The output from the system is then fed back to the sum block with a negative gain, forming a closed-loop negative feedback system. A step input of 10 radians is introduced into the system, and PID parameters, specifically K_p (proportional gain), K_d (derivative gain), and K_i (integral gain), were fine-tuned using the MATLAB's real-time PID auto-tuner, which relies on a system model-based approach, focusing on system response tuning and transient response tuning. After introducing the plant to the tuner, it linearizes the system in preparation for tuning. Finally, the optimal gains and the filter coefficient obtained from the toolbox are K_p=28.446, K_i=2.11, K_d=4.699 and N=118.794. These gain values are plugged into the Eq. (4) to form a PID controller.

In system response tuning, the system's rapid or gradual response to the input is considered a design parameter. In transient method tuning, the parameters of interest are the system's robustness and aggressiveness. Given the system's performance and response, the robustness and aggressiveness of the controller were adjusted to the anticipated level, and the relevant settings were applied. After achieving the desired system response, the tuning parameters and Filter Coefficient were extracted from the tuner. Saturation parameters were established to confine the output of the PID controllers within the maximum acceptable rating of the hardware, with an Upper Limit = +12 and Lower Limit = −12 [9].

$$u(t) = K_p e(t) + K_i \int_0^t e(t)dt + K_d \frac{de(t)}{dt} \tag{4}$$

where $u(t)$ represents the output of the controller and $e(t)$ represents the error signal from the reference point.

Closed-loop transfer function of the system is calculated by obtaining the Laplace transform for the Eq. (4) as shown in Eq. (5) and by plugging in Eq. (5) to Eq. (6). The stability analysis of the PID controller is performed by obtaining the ZPK representation of the closed-loop transfer function of the Eq. (6) as shown in the Eq. (7). From Eq. (7) it is observed the locations of closed-loop poles are lying on the left of the S-plane. So, the designed closed-loop system is stable.

$$C(s) = K_p + \frac{K_i}{s} + K_d \frac{N}{1 + N\frac{1}{s}} \tag{5}$$

$$\frac{Y(s)}{R(s)} = \frac{G(s)C(s)}{1 + G(s)C(s)} \tag{6}$$

$$\frac{3474(s + 5.689)(s + 0.07511)}{(s + 5.221)(s + 0.07481)(s^2 + 121.7s + 3800)} \tag{7}$$

where, C(s) is the controller transfer function, R(s) is the closed loop transfer function and G(s) is the plant transfer function given by Eq. (3).

2) DESIGN OF MPC CONTROLLER

The MPC is a modern, rapidly evolving, high-performance system known for its constraint satisfaction. However, because there is no defined way for tuning the controller parameters, creating an MPC controller is difficult. The prediction horizon (Np), control horizon (Nc), input constraints, weights, and sample time are among the parameters. We can change the system's performance parameters, such as the controller's robustness and aggressiveness, similarly to PID tuning. Furthermore, the MPC controller's state estimation response, which determines the system's weight, can be modified [17].

Initially, the MPC structure is defined with a single manipulated variable and a single input system. The physical system constraints are outlined in Table 4. The MPC parameters are tuned based on the closed-loop system behavior. First, a longer Np is selected and a nominal Nc is selected along with the input and output weights of the system. The behavior of the system is monitored and the parameters are fine-tuned manually. The rate weight on the input side is set at 0.01353, while the output weight is fixed at 7.3890. The system response was evaluated using various values for

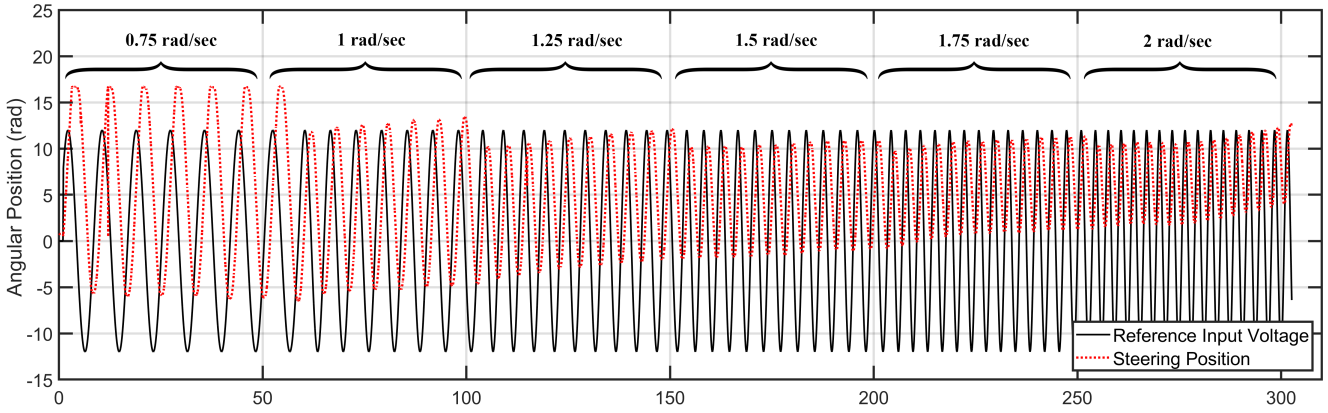

FIGURE 9. Frequency response modeling.

the prediction and control horizons. It is important to note that the system's robustness and stability increase with an increase in Np. However, beyond a certain Np value, further increases in this variable do not significantly impact the system. Conversely, when the control horizon (Nc) increases, the system's aggressiveness also increases, but at the expense of stability. In our case, the goal is to design a robust steering controller. As a compromise, the value of Np is set higher, Np=20 than the value of Nc, $Nc = 2$. This value of Nc is chosen according to the general rule, $0.1Np \leq Nc \leq 0.2Np$. The MPC's sampling time (Ts) is kept constant at Ts=0.001 seconds, playing a crucial role in the computational performance of the controller. These parameters are used to design the MPC controller in MATLAB and the overall representation and cost function of the MPC system in given in Eq. (8) and (9) respectively.

$$U_t^*(x(t)) = arg\min_{U_t} \sum_{k=0}^{N-1} q(x_{t+k}, u_{i(t+k)}) \tag{8}$$

where U_t represents the optimization variable, $x(t)$ is measurement, x_{t+k} is state constraints and $u_{i(t+k)}$ is input constraints of the systems.

$$J = \sum_{i=1}^{p} w_e e_{k+i^2} + \sum_{i=0}^{p-1} w_{\Delta u} \Delta u_{k+i^2} \tag{9}$$

where J represents the Cost function, w is weights of the system, e is error and Δu is controller action.

Closed-loop stability analysis of the MPC controller is determined by the root locus method by obtaining the total system's transfer function including the controller as discussed in Section III. From the obtained root locus it is observed the locations of closed-loop poles are lying on the left of the S-plane. So, the closed-loop system is said to be stable.

C. SIMULINK SETUP AND DATA ACQUISITION

1) PIN CONFIGURATION

All electrical connections between the Speedgoat target machine and the actual hardware are made through the Speedgoat's terminal board. The encoder section of the steering wheel provides high-frequency digital pulses as input to the system, while the steering's multi-turn potentiometer serves as the analog input. The steering wheel actuation is achieved through the Cytron motor, which requires high-frequency PWM digital signals as input. In the Simulink environment, these pins are configured as shown in Fig. 10. The Pin setup block is used to declare the analog and digital inputs and outputs. A sampling time of 0.0001 seconds is set for each block. The analog input to the system has a maximum sample rate of 200 kSPS and is equipped with an anti-aliasing filter with a −3 dB cutoff frequency. The digital I/O lines operate at a Low Voltage-TTL level of 3.3V with a 5V tolerance [29]

TABLE 4. MPC constraints.

Channel	Type	Min	Max	RateMin	RateMax
Input u(t)	MV	2	-12	12	+Inf
Output y(t)	MO	13	16	-	-

2) IMPLEMENTATION OF PD, PID, AND MPC CONTROLLERS

The PID block in Simulink simplifies the system by directly handling the steering's position error in radians. The PID output is limited to a range of −12V to +12V, as the input voltage to the steering motor is proportional to the position. Therefore, the PID controller's output serves as the motor voltage. To convert the voltage output from the PID controller to PWM values, a mapping is applied. A voltage of −12V corresponds to a PWM value of 0, while +12V corresponds to a PWM value of 1. For example, a PWM value of 0.5 results in 0V being applied to the steering motor. This mapping is based on the steering motor driver's datasheet and straight-line equation that is represented by Eqs. (10)–(12). The PD and the PID controller are implemented similarly, with the inclusion of the K_i term in the controller's gain. The control structure of PID implemented in the MATLAB Simulink is shown in Fig. 12. Fig. 11 shows the root locus for the designed PID closed loop system with the desired specifications. The

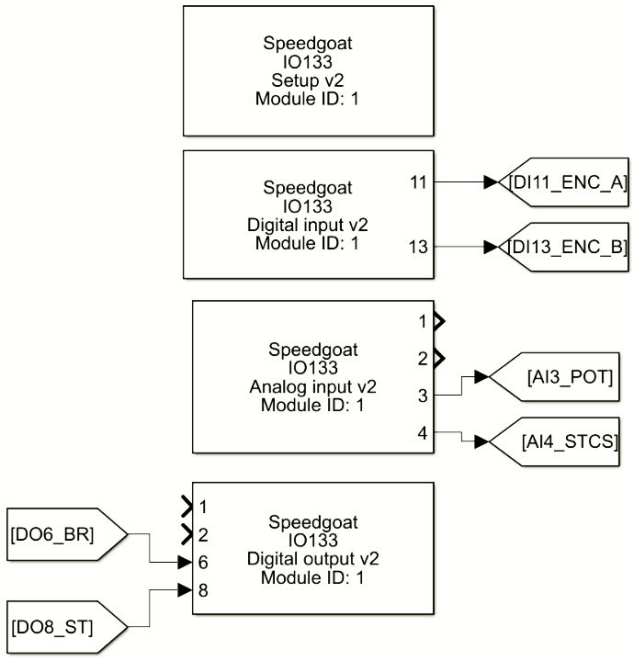

FIGURE 10. I/O configuration with HIL and Simulink.

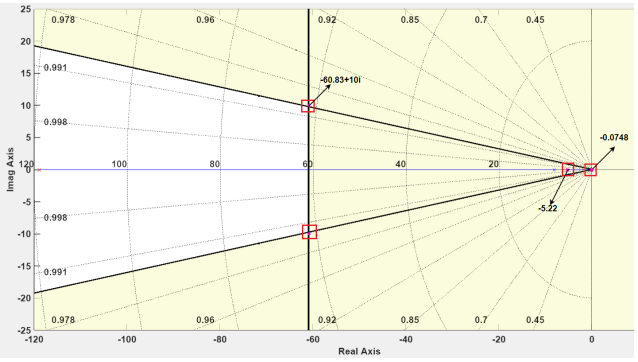

FIGURE 11. Root locus of the closed-loop PID system.

poles location of the root locus matches with the ZPK form of the closed-loop transfer function shown in Eq. (7).

To implement the MPC controller in Simulink, the actual steering position angle is directly fed into the measured output port of the MPC controller block. The desired steering position reference is provided to the controller's ref port. The manipulated variable, which ranges from −12V to 12V, is the output from the controller. This value is then converted to PWM values, as the motor driver requires PWM to actuate the motor [30]. The control structure of MPC implemented in the MATLAB Simulink is shown in Fig. 13.

$$\frac{y - y_1}{y_2 - y_1} = \frac{x - x_1}{x_2 - x_1} \tag{10}$$

$$\frac{y - 1}{0.5 - 1} = \frac{x - 12}{0 - 12} \tag{11}$$

$$y = 0.0416666(x) + 0.5 \tag{12}$$

where x represents the output voltage from the designed controller, and y represents the steering motor driver's input PWM signal.

3) DATA ACQUISITION

All data from each block is logged using Simulink Data Inspector with a sampling time of 0.0001 seconds. The Speedgoat performance target machine ensures accurate and high-resolution logging of data. Analog data is recorded with a 16-bit resolution. The Simulink Data Inspector allows real-time inspection of captured data and enables comparison with time series data at multiple stages and runs simultaneously.

IV. EXPERIMENTAL RESULTS AND DISCUSSION

The robustness of each controller is analysed by how well the controller can maintain at the given setpoint, when the vehicle travels in a speed breaker. The results were obtained for two different vehicle speeds along the power consumption of each controller.

1) CLOSED-LOOP CONTROLLER'S STEERING PERFORMANCE IN JACKED POSITION

The vehicle's front wheels are lifted using two hydraulic jacks, and the closed response was logged. The experimental and simulated results for PD, PID, and MPC controllers, along with the power consumed by the controller drive system, are shown in Fig. 14 (a), (b), and (c), respectively.

It was observed that the MPC controller outperformed the PD and PID controllers with a shorter settling time and a steady-state error of less than 1%. The power consumed by the MPC control drive was also lower compared to the other controllers. The PD controller performed better than the PID controller because the steering system had a constant error, and the integral term of the PID controller added up the error, making the controller system unstable. This constant steady-state error and high-power consumption are the reasons behind the performance of the PID controller. The simulated results matched the experimental results perfectly, validating the design of the PD, PID, and MPC controllers.

A. OPEN-LOOP RESPONSE

The behavior of the steering is logged for the open-loop steering system. The results obtained for two different velocities, 1 km/h and 2 km/h, are shown in Fig. 15 (a) and (b), respectively.

The displacement of the steering at 1 km/h is significantly smaller compared to the displacement at 2 km/h. A robust controller must be developed to maintain the steering at the respective angle, even when the vehicle encounters external disturbances such as speed bumps, debris, and rough terrain.

B. REAL-TIME TESTING OF CLOSED-LOOP CONTROLLERS PERFORMANCE WITH DIFFERENT SAMPLING TIMES

1) SAMPLING TIME OF THE CONTROLLER - 0.001 SEC

Closed loop responses with PD, PID, and MPC controllers were logged using Simulink data inspector for two different velocities, 1 km/h and 2 km/h. Fig. 16 (a) and (b) depict the closed-loop response and power consumption of the PD controller at these velocities.

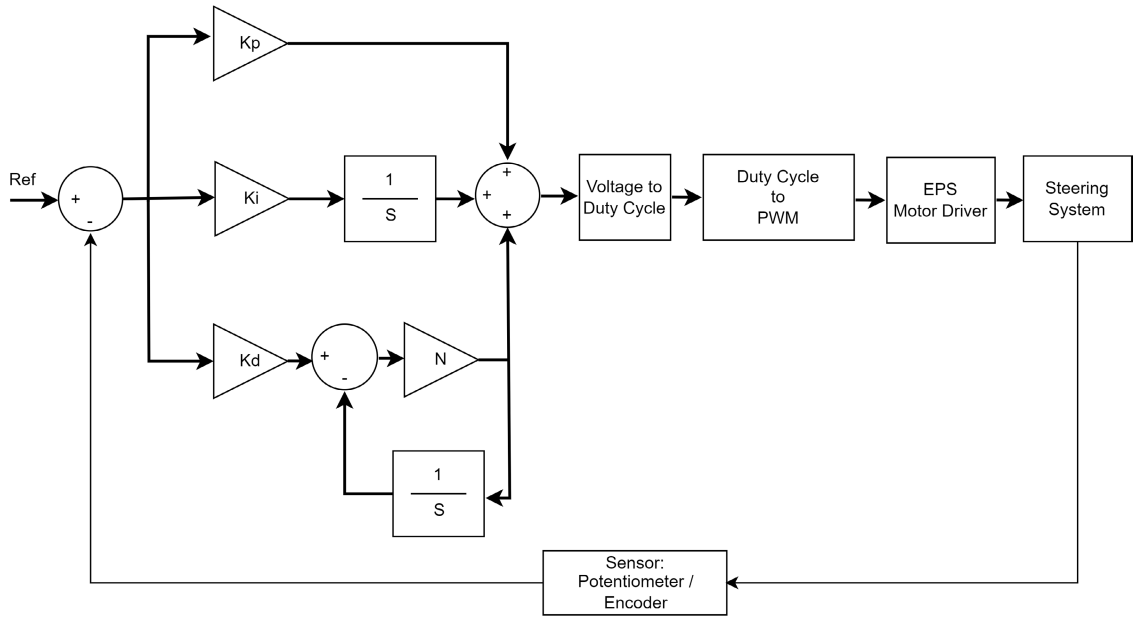

FIGURE 12. PID controller implementation.

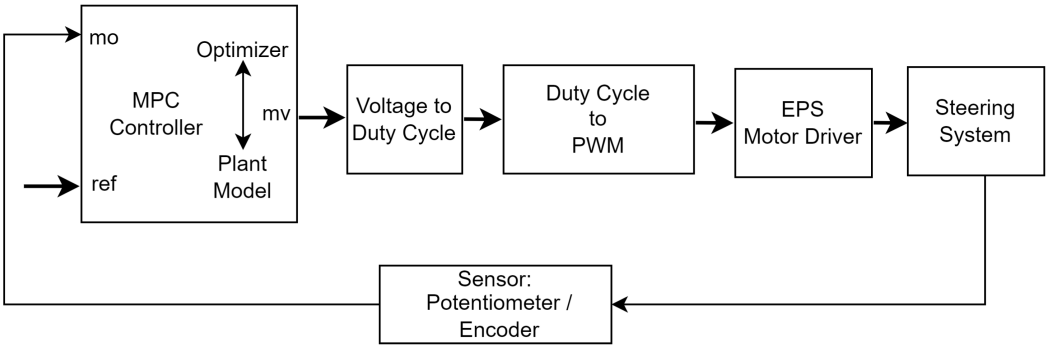

FIGURE 13. MPC controller implementation.

At 1 km/h, the PD controller exhibits decent response; however, at 2 km/h, the PD controller loses its robustness and the response deviates. The power consumption remains similar and constant for both velocities, with a maximum requirement of approximately 40 watts and an average requirement of around 15 watts. The closed-loop response and power consumption of the PID controller are illustrated in Fig. 17 (a) and (b) respectively.

The response of the PID controller, at a speed of 1 km/h, has effectively maintained the steering position with a maximum displacement of 0.1 radians. The controller's performance remains consistent even as the speed increases to 2 km/h. Power consumption at these two speeds is similar and constant. The peak power requirement is approximately 25 watts, with an average requirement of around 8 watts. The closed-loop response of the MPC controller and its power consumption are shown in Fig. 18 (a) and (b), respectively, at two different velocities.

The MPC controller exhibits significant instability, particularly at the lower speed of 1 km/h. Additionally, the power consumed by the MPC controller is high, with a maximum demand of around 60 watts and an average of approximately 25 watts. This instability is primarily caused by small disturbances on the steering wheels due to the irregular terrain of the road surface. Generally, the MPC controller requires an accurately modeled system with included disturbances, which necessitates estimating complex model coefficients.

2) SAMPLING TIME OF THE CONTROLLER - 0.002 SEC

The initial sampling time in the closed-loop response for all the controllers was set to 0.001 seconds. Since the sampling time depends on the microcontroller used in the actual system, it is important to vary the sampling time and validate performance. The sampling time for PD, PID, and MPC controllers was increased to 0.002 seconds, and the results were obtained at a constant speed of 1 km/h. The results,

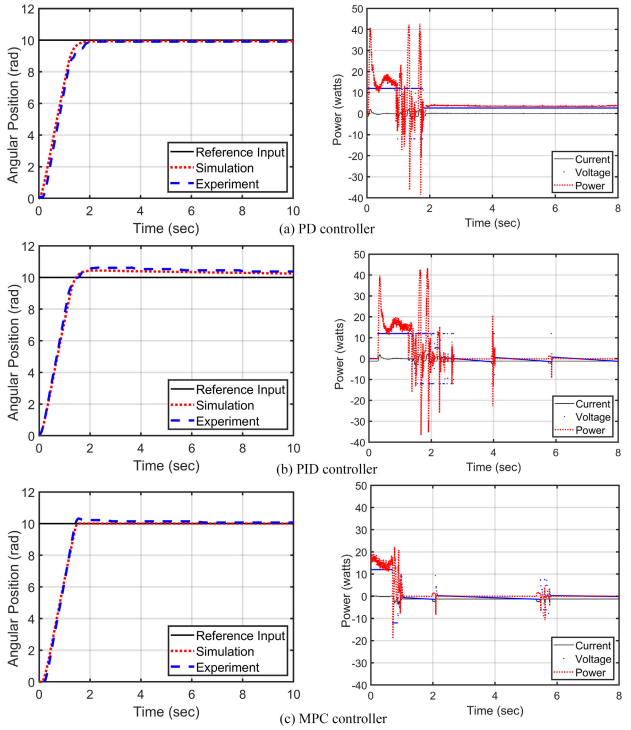

FIGURE 14. Validation of experimental (Jacked) and simulation performance of different controllers for the steering system and their control input.

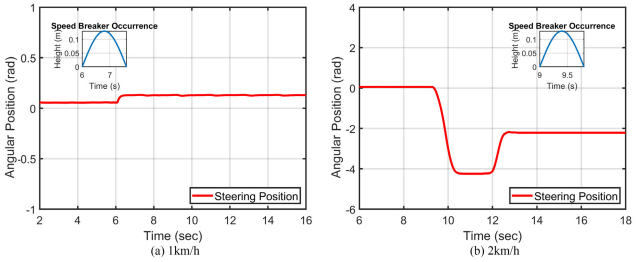

FIGURE 15. Open-loop response.

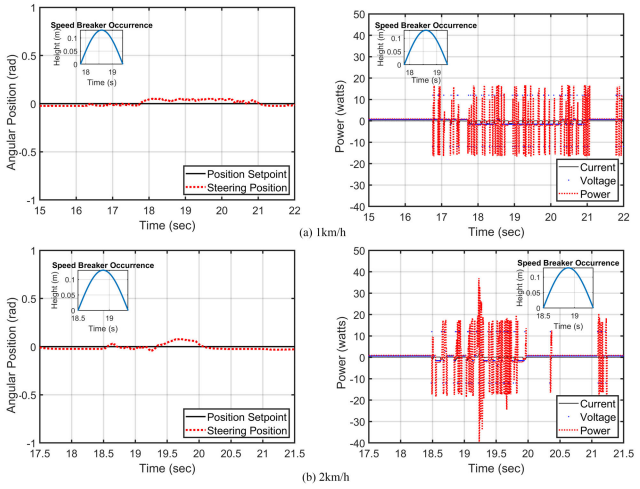

FIGURE 16. Steering angular position and control input of PD controller with different vehicle speeds.

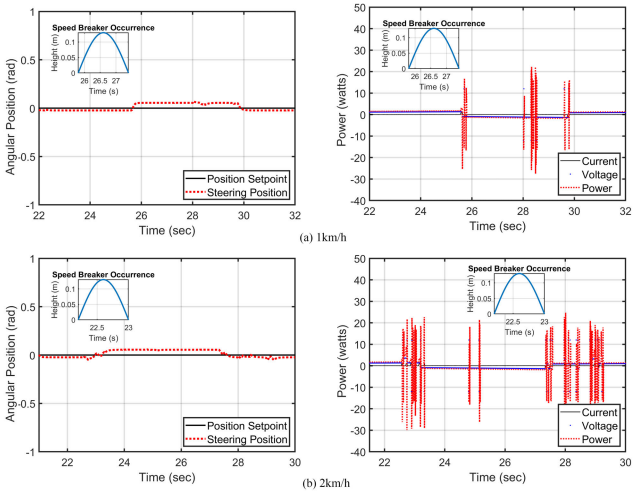

FIGURE 17. Steering angular position and control input of PID controller with different vehicle speeds.

showing the power consumed by the controller drive system with the PD, PID, and MPC controllers, are presented in Fig. 19 (a), (b), and (c) respectively.

The above results indicate that increasing the sampling time decreases the performance of all the controllers and increases the power consumption of the drive system. Compared to MPC, the performance of the PD and PID controllers is significantly poorer at higher sampling rates.

- Results demonstrated that the MPC controller surpassed the PD and PID controllers in jack response, exhibiting better performance and lower power consumption. While the PD controller had a steady state error below 1% but a longer rise time than the MPC, the PID controller experienced a steady state error exceeding 2%.
- During on-road testing at 1 km/h, all controllers aimed to maintain a reference position of 0 rad. The PD controller achieved an error of less than 1%, the PID controller performed with an error below 2%, and the MPC controller struggled with stability due to constant disturbances. Power consumption was lowest for the PID controller in this scenario compared to the PD and MPC controllers.
- At 2 km/h, the PID controller outperformed the PD controller, which experienced instability initially but eventually recovered. The MPC controller exhibited unstable responses but improved compared to the 1 km/h results. Power consumption remained lower for the PID controller when compared to the PD and MPC controllers.
- At 1 km/h with an increased sampling rate of 0.002 sec, the MPC controller excelled compared to the PD and PID controllers, which lost stability. The MPC controller maintained superior power consumption compared to

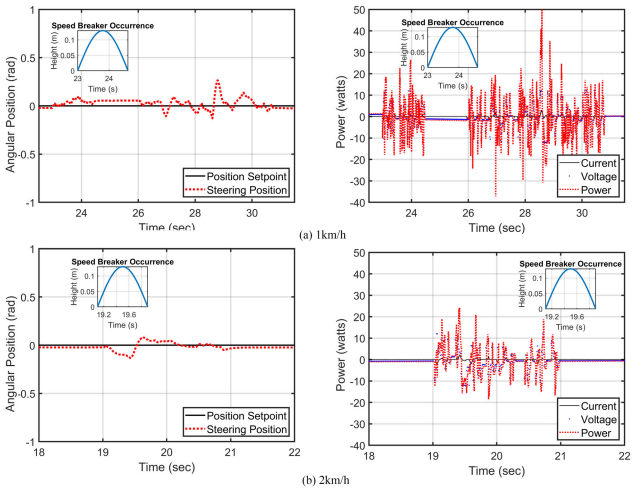

FIGURE 18. Steering angular position and control input of MPC controller with different vehicle speeds.

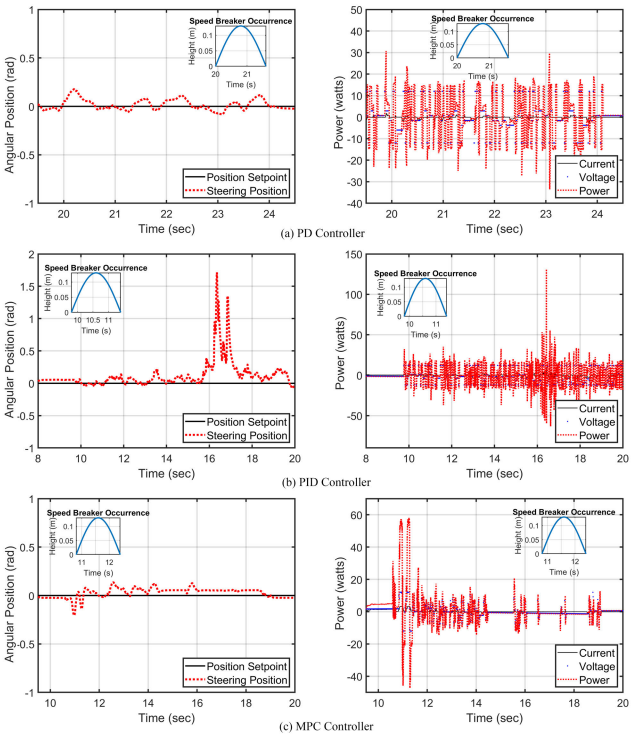

FIGURE 19. Steering angular position and control input of different controllers with speed as 1 km/h and sampling time of 0.002 seconds.

the PD and PID controllers, with the PID controller peaking at 140 Watts due to instability.

V. CONCLUSION

The study compared PD, PID, and MPC controllers for the autonomous vehicle's steering system using real-time data obtained from the HIL machine in a real modified electric car under various test scenarios. The results highlighted the strengths and weaknesses of each controller. The MPC controller demonstrated superior tracking performance in the absence of external disturbances. The PD controller exhibited robustness against constant small disturbances, while the PID controller performed well in the presence of impulse disturbances. Power consumption varied among the controllers, with the MPC controller consistently consuming less power. Overall, the choice of controller depends on the specific requirements and the ability to model external disturbances.

Future research in autonomous vehicle development can focus on advanced control algorithms beyond PD, PID, and MPC controllers to enhance steering system performance. Sensor fusion and perception can be explored to integrate multiple sensors for improved accuracy. Safety measures and redundancy mechanisms should be developed to ensure fail-safe operation. Real-world testing and validation in various driving scenarios can provide a comprehensive evaluation. Human-machine interaction aspects, including driver behavior and interaction interfaces, should be studied for seamless collaboration. These research directions aim to advance steering system performance, improve safety, and enhance the overall development of autonomous vehicles.

ACKNOWLEDGMENT

The authors would like to thank Team AutoZ and Vellore Institute of Technology for providing the required facilities and necessary support to complete the concerned work.

REFERENCES

[1] T. M. Vu, R. Moezzi, J. Cyrus, and J. Hlava, "Model predictive control for autonomous driving vehicles," *Electronics*, vol. 10, no. 21, p. 2593, Oct. 2021.

[2] L. Tang, F. Yan, B. Zou, K. Wang, and C. Lv, "An improved kinematic model predictive control for high-speed path tracking of autonomous vehicles," *IEEE Access*, vol. 8, pp. 51400–51413, 2020.

[3] H. Nam, W. Choi, and C. Ahn, "Model predictive control for evasive steering of an autonomous vehicle," *Int. J. Automot. Technol.*, vol. 20, no. 5, pp. 1033–1042, Aug. 2019.

[4] C. Sun, X. Zhang, L. Xi, and Y. Tian, "Design of a path-tracking steering controller for autonomous vehicles," *Energies*, vol. 11, no. 6, p. 1451, Jun. 2018.

[5] S. Xu and H. Peng, "Design, analysis, and experiments of preview path tracking control for autonomous vehicles," *IEEE Trans. Intell. Transp. Syst.*, vol. 21, no. 1, pp. 48–58, Jan. 2020.

[6] J. Wu, J. Zhang, Y. Tian, and L. Li, "A novel adaptive steering torque control approach for human–machine cooperation autonomous vehicles," *IEEE Trans. Transport. Electrific.*, vol. 7, no. 4, pp. 2516–2529, Dec. 2021.

[7] Y. W. Jeong, C. C. Chung, and W. Kim, "Nonlinear hybrid impedance control for steering control of rack-mounted electric power steering in autonomous vehicles," *IEEE Trans. Intell. Transp. Syst.*, vol. 21, no. 7, pp. 2956–2965, Jul. 2020.

[8] M. Huang, W. Gao, Y. Wang, and Z.-P. Jiang, "Data-driven shared steering control of semi-autonomous vehicles," *IEEE Trans. Human-Mach. Syst.*, vol. 49, no. 4, pp. 350–361, Aug. 2019.

[9] S.-P. Chen, G.-M. Xiong, H.-Y. Chen, and D. Negrut, "MPC-based path tracking with PID speed control for high-speed autonomous vehicles considering time-optimal travel," *J. Central South Univ.*, vol. 27, no. 12, pp. 3702–3720, Dec. 2020.

[10] Q. Cui, R. Ding, X. Wu, and B. Zhou, "A new strategy for rear-end collision avoidance via autonomous steering and differential braking in highway driving," *Vehicle Syst. Dyn.*, vol. 58, no. 6, pp. 955–986, Apr. 2019.

[11] A. Kirli, Y. Chen, C. E. Okwudire, and A. G. Ulsoy, "Torque-vectoring-based backup steering strategy for steer-by-wire autonomous vehicles with vehicle stability control," *IEEE Trans. Veh. Technol.*, vol. 68, no. 8, pp. 7319–7328, Aug. 2019.
[12] C. Zhang, J. Hu, J. Qiu, W. Yang, H. Sun, and Q. Chen, "A novel fuzzy observer-based steering control approach for path tracking in autonomous vehicles," *IEEE Trans. Fuzzy Syst.*, vol. 27, no. 2, pp. 278–290, Feb. 2019.
[13] H. Saleem, F. Riaz, L. Mostarda, M. A. Niazi, A. Rafiq, and S. Saeed, "Steering angle prediction techniques for autonomous ground vehicles: A review," *IEEE Access*, vol. 9, pp. 78567–78585, 2021.
[14] J. Loof, I. Besselink, and H. Nijmeijer, "Automated lane changing with a controlled steering-wheel feedback torque for low lateral acceleration purposes," *IEEE Trans. Intell. Vehicles*, vol. 4, no. 4, pp. 578–587, Dec. 2019.
[15] P. Hang and X. Chen, "Towards autonomous driving: Review and perspectives on configuration and control of four-wheel independent drive/steering electric vehicles," *Actuators*, vol. 10, no. 8, p. 184, Aug. 2021.
[16] N. Ahmadian, A. Khosravi, and P. Sarhadi, "Integrated model reference adaptive control to coordinate active front steering and direct yaw moment control," *ISA Trans.*, vol. 106, pp. 85–96, Nov. 2020.
[17] N. Awad, A. Lasheen, M. Elnaggar, and A. Kamel, "Model predictive control with fuzzy logic switching for path tracking of autonomous vehicles," *ISA Trans.*, vol. 129, pp. 193–205, Oct. 2022.
[18] Q. Li and X. Li, "Trajectory planning for autonomous modular vehicle docking and autonomous vehicle platooning operations," *Transp. Res. E, Logistics Transp. Rev.*, vol. 166, Oct. 2022, Art. no. 102886.
[19] W. Zhang, "A robust lateral tracking control strategy for autonomous driving vehicles," *Mech. Syst. Signal Process.*, vol. 150, Mar. 2021, Art. no. 107238.
[20] S. Cheng, L. Li, X. Chen, J. Wu, and H.-d. Wang, "Model-predictive-control-based path tracking controller of autonomous vehicle considering parametric uncertainties and velocity-varying," *IEEE Trans. Ind. Electron.*, vol. 68, no. 9, pp. 8698–8707, Sep. 2021.
[21] Z. Luan, J. Zhang, W. Zhao, and C. Wang, "Trajectory tracking control of autonomous vehicle with random network delay," *IEEE Trans. Veh. Technol.*, vol. 69, no. 8, pp. 8140–8150, Aug. 2020.
[22] S. Cheng, L. Li, C.-Z. Liu, X. Wu, S.-N. Fang, and J.-W. Yong, "Robust LMI-based H-infinite controller integrating AFS and DYC of autonomous vehicles with parametric uncertainties," *IEEE Trans. Syst. Man, Cybern. Syst.*, vol. 51, no. 11, pp. 6901–6910, Nov. 2021.
[23] Q. Yao, Y. Tian, Q. Wang, and S. Wang, "Control strategies on path tracking for autonomous vehicle: State of the art and future challenges," *IEEE Access*, vol. 8, pp. 161211–161222, 2020.
[24] A. Amini, I. Gilitschenski, J. Phillips, J. Moseyko, R. Banerjee, S. Karaman, and D. Rus, "Learning robust control policies for end-to-end autonomous driving from data-driven simulation," *IEEE Robot. Autom. Lett.*, vol. 5, no. 2, pp. 1143–1150, Apr. 2020.
[25] H. Pang, R. Yao, P. Wang, and Z. Xu, "Adaptive backstepping robust tracking control for stabilizing lateral dynamics of electric vehicles with uncertain parameters and external disturbances," *Control Eng. Pract.*, vol. 110, May 2021, Art. no. 104781.
[26] H. He, M. Shi, J. Li, J. Cao, and M. Han, "Design and experiential test of a model predictive path following control with adaptive preview for autonomous buses," *Mech. Syst. Signal Process.*, vol. 157, Aug. 2021, Art. no. 107701.
[27] S. R. Kakarlapudi and R. Sultana, "Design of digital twin for safety systems in electric vehicles," in *Proc. Int. Conf. Next Gener. Electron. (NEleX)*, Dec. 2023, pp. 1–6.
[28] D. Łuczak, "Nonlinear identification with constraints in frequency domain of electric direct drive with multi-resonant mechanical part," *Energies*, vol. 14, no. 21, p. 7190, Nov. 2021.
[29] S. Carpiuc, "Model–based control and real–time simulation of a four–phase PMSM traction drive," in *Proc. Int. Conf. Electr. Mach. (ICEM)*, Sep. 2022, pp. 2378–2383.
[30] M. Larrea, E. Irigoyen, F. Artaza, and V. Gómez-Garay, *Model-Based Design IMO-NMPC Strategy: Real-Time Implementation*. Cham, Switzerland: Springer, 2023, pp. 71–81.

S. GOKUL KRISHNAN is currently pursuing the B.Tech. degree in electrical engineering with Vellore Institute of Technology (VIT University), Vellore. He is also a Visiting Research Intern with the King Abdullah University of Science and Technology (KAUST), Saudi Arabia, working on future smart DC grid technologies. Previously, he was a Research Intern with Indian Institute of Space Science and Technology (IIST-ISRO), Thiruvananthapuram, where he was developed the electrical power systems (EPS) for small satellites. He is also an Undergraduate Researcher with the Automotive Research Center (ARC), VIT. His research interests include modern grid-connected power electronics, power systems, control systems, hardware-in-the-loop (HIL), and rapid control prototyping (RCP) systems.

P. SURESH KUMAR received the master's degree from NIT Trichy and the Ph.D. degree in design of control systems from Indian Institute of Space Science and Technology (IIST-ISRO). He is currently an Assistant Professor with the Autonomous Vehicles Research Laboratory, Automotive Research Center (ARC), Vellore Institute of Technology (VIT University), Vellore. With a strong background in modeling and controller design, he has published extensively in renowned scientific journals and presented his research at international conferences. His expertise lies mainly in autonomous aerial, ground vehicles, and electric vehicles. He actively engages in interdisciplinary collaborations, in cutting-edge research projects.

NADHEEM NASSAR MATARA is currently pursuing the B.Tech. degree in mechanical engineering and in automotive engineering with Vellore Institute of Technology (VIT University), Vellore. He has played a role in Defense Research and Development Organization (DRDO) funded projects, specifically contributing to the development of a multifunctional rover for antitank landmine detection. He is also an Undergraduate Researcher with the Automotive Research Center (ARC), VIT. His profound expertise in the domains of automotive safety system, generative design, additive manufacturing, computer-aided simulation, and finite element analysis (FEA). These proficiencies underscore a multifaceted skill set, positioning him at the intersection of theoretical knowledge and hands-on application.

YONG WANG received the Ph.D. degree in energy and power engineering from Huazhong University of Science and Technology, China, in 2010, and the Ph.D. degree in industrial engineering and operations research from the University of Illinois at Chicago, in 2015. He was a Visiting Scholar with the Department of Mechanical Engineering, University of Michigan, Ann Arbor (2007–2009). He is currently an Associate Professor with the Department of Systems Science and Industrial Engineering, Watson College of Engineering and Applied Science, Binghamton University. His research with Binghamton University focuses on the design, modeling, and management of complex systems (energy, healthcare, manufacturing, and transportation).